

Nanoscale

Accepted Manuscript



This is an *Accepted Manuscript*, which has been through the Royal Society of Chemistry peer review process and has been accepted for publication.

Accepted Manuscripts are published online shortly after acceptance, before technical editing, formatting and proof reading. Using this free service, authors can make their results available to the community, in citable form, before we publish the edited article. We will replace this *Accepted Manuscript* with the edited and formatted *Advance Article* as soon as it is available.

You can find more information about *Accepted Manuscripts* in the [Information for Authors](#).

Please note that technical editing may introduce minor changes to the text and/or graphics, which may alter content. The journal's standard [Terms & Conditions](#) and the [Ethical guidelines](#) still apply. In no event shall the Royal Society of Chemistry be held responsible for any errors or omissions in this *Accepted Manuscript* or any consequences arising from the use of any information it contains.



Selective photochemical synthesis of Ag nanoparticles on position-controlled ZnO nanorods for the enhancement of yellow-green light emission

Received 00th January 20xx,
Accepted 00th January 20xx

DOI: 10.1039/x0xx00000x

www.rsc.org/

Hyeong-Ho Park,^{‡*a} Xin Zhang,^{‡b} Keun Woo Lee,^c Ahrum Sohn,^d Dong-Wook Kim,^d Joondong Kim,^e Jin-Won Song,^f Young Su Choi,^c Hee Kwan Lee,^c Sang Hyun Jung,^a In-Geun Lee,^{a,g} Young Dae Cho,^{a,g} Hyun-Beom Shin,^c Ho Kun Sung,^c Kyung Ho Park,^a Ho Kwan Kang,^a Won-Kyu Park^a and Hyung-Ho Park^g

A novel technique for the selective photochemical synthesis of silver (Ag) nanoparticles (NPs) on ZnO nanorod arrays is established, by combining ultraviolet-assisted nanoimprint lithography (UV-NIL) for the definition of growth sites, hydrothermal reaction for the position-controlled growth of ZnO nanorods, and photochemical reduction for the decoration of Ag NPs on the ZnO nanorods. During photochemical reduction, the size distribution and loading of Ag NPs on ZnO nanorods can be tuned by varying the UV-irradiation time. The photochemical reduction is hypothesized to facilitate the adsorbed citrate ions on the surface of ZnO, allowing Ag ions to preferentially form Ag NPs on ZnO nanorods. The ratio of visible emission to ultraviolet (UV) emission for the Ag NPs-decorated ZnO nanorod arrays, synthesized for 30 min, is 20.5 times of that for the ZnO nanorod arrays without Ag NPs. The enhancement of the visible emission is believed to associate with the surface plasmon (SP) effect of Ag NPs. The Ag NPs-decorated ZnO nanorod arrays show significant SP-induced enhancement of yellow-green light emission, which could be useful in optoelectronic applications. The technique developed here requires low processing temperatures (120 °C and lower) and no high-vacuum deposition tools, suitable for applications such as flexible electronics.

Introduction

Semiconductor-metal multicomponent complex structures exhibit interesting optical properties: tunable spectral response, high responsivity, and improved light emission.¹⁻⁴ Among many semiconductor structures, one-dimensional (1D) zinc oxide (ZnO) nanostructures, together with their derived multicomponent complex structures, are of great interest for the development of devices in various fields, such as light emitting diodes,^{5,6} solid state lasers,^{7,8} energy harvesting,^{9,10} chemical sensing^{11,12} and plasmonic devices.^{13,14}

To fabricate devices using 1D nanostructures such as nanorods and nanowires, the integration of these nanostructures in device structures can be challenging. For example, free standing nanorods would require additional manipulation to integrate them into device structures, where lithography and etch steps are commonly used. These steps could alter nanorod properties and thus add more variables in device reliability. Therefore, it is desired for the following device fabrication that the nanorods can be prepared on a substrate with controllable positioning, sizes and even quality.

Silver (Ag) is well known for exhibiting prominent response to electromagnetic fields because of its strong surface plasmon resonance (SPR), which is induced by the resonant oscillation of surface electrons when illuminated with light of appropriate wavelength.¹⁵ Ag nanoparticles (NPs)-decorated ZnO nanorods, with enhanced optical, electrical, and antimicrobial properties,^{16,17} potentially useful for compact light sources, energy harvesting and chemical sensing devices,^{18,19} may represent a promising class of functional hybrid composite materials, since the coupling between Ag NPs and ZnO nanorods could induce novel hybrid properties. It is expected that the variation in the size distribution of Ag NPs in the ZnO matrix would significantly affect the interactions between the composite material and the incident light, and thus the induced properties. Therefore, in this paper we investigated the photoluminescence of position-controlled ZnO nanorods

^a Technology Development Division, Korea Advanced Nanofab Center (KANC), Suwon 443270, Korea. Fax: +82 31 546 6409; Tel: +82 31 546 6217; E-mail: hyeongho.park@kanc.re.kr

^b Department of Chemistry and 4D LABS, Simon Fraser University, Burnaby, BC, V5A 1S6, Canada

^c Nano Process Division, Korea Advanced Nanofab Center (KANC), Suwon 443270, Korea

^d Department of Physics, Ewha Womans University, Seoul 120750, Korea

^e Department of Electrical Engineering, Incheon National University, Incheon 406772, Korea

^f Research Institute, Ecoflux Co. Ltd, Cheongju 363911, Korea

^g Department of Materials Science and Engineering, Yonsei University, Seoul, 120749, Korea

‡ These authors equally contributed to this work.

* Electronic Supplementary Information (ESI) available: Quantitative analyses of Ag NPs-decorated ZnO nanorods resulted from different UV-irradiation times. See DOI: 10.1039/x0xx00000x

decorated with Ag NPs at different Ag loadings and size distributions.

Various methodologies have been reported to prepare Ag NPs-decorated ZnO of different architectures. Some typical examples include incorporating Ag NPs into ZnO nanofibers through electrospinning,²⁰ doping Ag into a ZnO thin film *via* pneumatic spray pyrolysis technique,²¹ obtaining worm-like Ag-ZnO hybrids through ultrasonic irradiation,²² and depositing Ag NPs on nanorods *via* photochemical deposition,²³ plasma enhanced chemical vapor deposition,²⁴ electrodeposition,²⁵ seed-mediated method,²⁶ or electron beam evaporation.²⁷ Among the above-mentioned, the photochemical route is a method that is relatively more cost-effective, easy to operate, suitable for flexible substrates due to its milder processing conditions (e.g. room temperature and requiring no vacuum system), and also possible to achieve selective deposition.

In our previous study, we demonstrated a novel technique for realizing position-controlled ZnO nanorods on an arbitrary substrate with a directly patterned seed layer *via* ultraviolet-assisted nanoimprint lithography (UV-NIL).²⁸ In this study, by simply introducing an additional photochemical deposition step, we have achieved the decoration of Ag NPs on position-controlled ZnO nanorods. It was found that in the photochemical step Ag NPs preferentially form on the ZnO nanorods. And the Ag loading on ZnO and the size distribution of Ag NPs can be tuned by varying the deposition time. These observations lend the technique demonstrated here a great potential to its application in the industrial mass production. In addition, the nanostructure, crystallinity, and photoluminescence of the Ag-ZnO composites prepared with various Ag loadings were also studied and discussed in this paper.

Experimental section

Position-controlled growth of ZnO nanorods on directly patterned ZnO seeds

As demonstrated in our previous work, position-controlled ZnO nanorods was prepared on directly patterned ZnO seeds *via* UV-NIL.²⁸ A silicon master consisting of line-space gratings of 1000 nm pitch, where the lines are 200 nm wide and 300 nm high, was used to replicate a flexible polyurethane acrylate (PUA) mold by UV imprinting procedure described elsewhere.^{29,30}

The p-Si (100) substrates to be used for the growth of ZnO nanorods were immersed in an acetone bath under sonication for 5 min, followed by an immersion in isopropyl alcohol for 5 min and rinsed with de-ionized (DI) water (Milli-Q, Millipore Corp.) for 3 min. Then, the Si substrates were cleaned in a 1:10 (V/V) dilute HF solution for 1 min to remove the native oxide and rinsed with DI water for 3 min. The substrates were dried under a nitrogen flow.

A photosensitive ZnO sol-gel precursor solution (0.25 M) was spin-coated on a cleaned p-Si (100) substrate to form a film. The film was baked on a hot plate (80 °C, 2 min) to remove residual solvent. The replicated PUA mold was then

pressed against the film (20 bar, room temperature) for 5 min, using a NIL-8 imprinter (Obducat, Sweden), followed by a UV light irradiation (25 mW cm⁻², 365 nm) for 7 min to induce photochemical reaction in the film. By detaching the PUA mold from the irradiated film, a Zn-containing pattern was obtained with a residual layer (~10 nm) between the imprinted features. After removing this residual layer by etching with Cl₂ gas in a plasma asher (TCP9408, 10 mTorr, 200 W, 45 s), the pattern was baked (120 °C, 1 h) in an oven to avoid loss of the pattern in an aqueous solution during the following hydrothermal growth.

Hydrothermal growth of ZnO nanorods was achieved by immersing a sample with its ZnO seed pattern facing down in a glass beaker filled with an aqueous growth solution (200 ml, 6 mM zinc nitrate [Zn(NO₃)₂·6H₂O, Sigma-Aldrich, 98%], 6 mM hexamethylenetetramine (HMT) [C₆H₁₂N₄, Sigma-Aldrich, 99.5%]). The reaction baker was covered with aluminium foil and then heated in a laboratory oven (70 °C, 5 h). After reaction, the sample was removed from the growth solution, rinsed with deionized water and dried by a N₂ flow.

Photochemical synthesis of Ag NPs on position-controlled ZnO nanorods

Photochemical synthesis of Ag NPs was conducted by immersing the sample with its ZnO nanorods facing up in a Pyrex glass petri dish filled with an aqueous solution made by mixing 25 ml 0.25 mM silver nitrate [AgNO₃, Sigma-Aldrich, 99%] with 25 ml 0.25 mM trisodium citrate dihydrate [HOC(COONa)(CH₂COONa)₂·2H₂O, Sigma-Aldrich, 99%] at room temperature. The sample and solution were irradiated under a UV light (25 mW cm⁻², 365 nm) for various reaction times between 0 and 45 min. During the UV-irradiation, the photochemical reduction dish was covered with another dish to prevent evaporation of the aqueous solution. Fig. 1 shows a

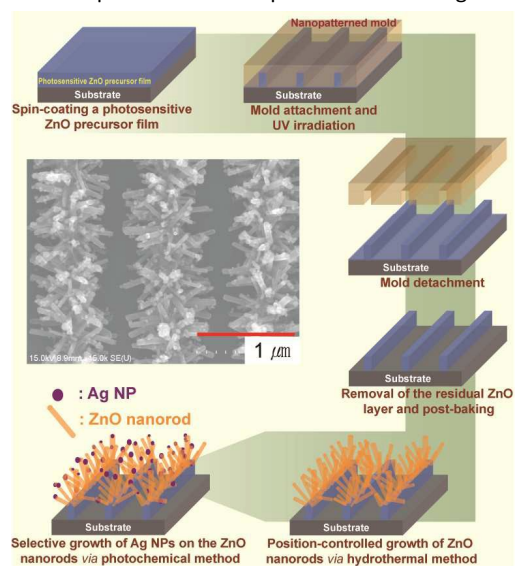


Fig. 1 Schematic diagram of the novel technique for the fabrication of Ag NPs-decorated ZnO nanorod arrays by combining UV-NIL for the definition of growth sites, hydrothermal reaction for the position-controlled growth of ZnO nanorods, and photochemical reduction for the decoration of Ag NPs on the ZnO nanorods.

schematic diagram of the above-described novel technique for the photochemical synthesis of Ag NPs on position-controlled ZnO nanorods by combining UV-NIL with hydrothermal growth.

Characterization

Morphology of the Ag NPs decorated ZnO nanorod arrays was examined using a Hitachi S-4800 field-emission scanning electron microscope (SEM). UV-visible spectra of the Ag precursor solution at different irradiation times were recorded with a Varian Cary 5000 UV-Vis-NIR spectrophotometer. The microstructure and crystallinity of Ag NPs and ZnO nanorods were investigated by transmission electron microscopy (TEM, JEM-2100F, JEOL, Japan). To prepare a TEM sample, the Ag NPs decorated ZnO nanorods were mechanically scratched off the substrate and dispersed on a TEM copper grid with holey carbon film support. The crystallinity of samples was investigated by X-ray diffraction (XRD) using a Rigaku D/Max 2500 diffractometer with a Cu K α radiation ($\lambda = 1.54178 \text{ \AA}$), operated at 40 kV and 300 mA. The photoluminescence (PL) measurements were performed using a PL mapping system (RPM 2000, Accent Optics, Denver, CO, USA) with a laser source emitting at the wavelength of 266 nm at room temperature.

Results and discussion

UV-Vis-NIR spectroscopy is a convenient method for detecting the formation of Ag NPs in Ag precursor solution. Specific signature peaks can be used to extract information on the size distribution of the Ag NPs.³¹ UV-visible spectra of the Ag precursor solutions were measured at different UV-irradiation times in the range of 250–900 nm, and the results are given in Fig. 2. After UV-irradiation of the precursor solution for 5 min, the appearance of a plasmon peak at ~ 420 nm indicated the formation of Ag NPs.³¹ By irradiating the precursor solutions with UV for 15, 30 and 45 min, the values of the wavelength at the maximum absorption (λ_{max}) were 429, 433, and 445 nm, respectively. It is reported that the UV-visible absorption spectrum of Ag NPs is associated with their size distribution.³¹ The wavelength at the λ_{max} increases as the average size of Ag NPs increases. The full width at half maximum (FWHM) reflects dispersity of the NPs, where a larger FWHM is attributed to a broader size polydispersity. In Fig. 2, the change in spectra evidences the increase of average particle size and the broader polydispersity of the Ag NPs due to the increasing UV-irradiation time. These results mean that the size distribution of Ag NPs can be tuned by UV-irradiation time during a photochemical reduction.

Fig. 3a shows the top-view SEM images of ZnO nanorod arrays on p-Si (100). From Fig. 3a, the average diameter and length of ZnO nanorods were found to be 58 and 294 nm, respectively. The growth mechanism of ZnO nanorods using the hydrothermal method has been well discussed in the literature.^{32,33} Hexamethylenetetramine (HMT) is a highly water soluble, non-ionic tetradentate cyclic tertiary amine. Thermal degradation of HMT releases NH $_3$ that reacts with

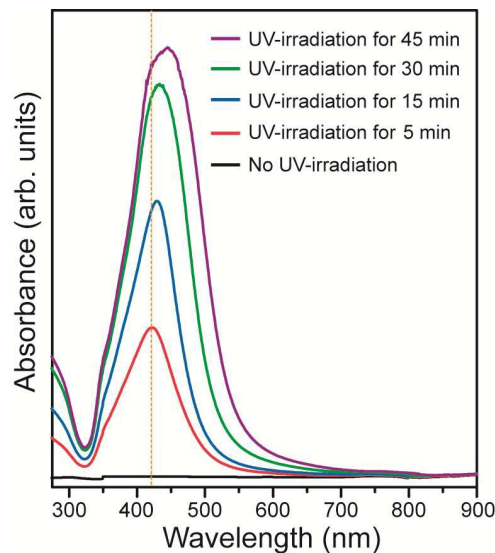


Fig. 2 UV-visible absorption spectra of the Ag colloidal solutions with different UV-irradiation times.

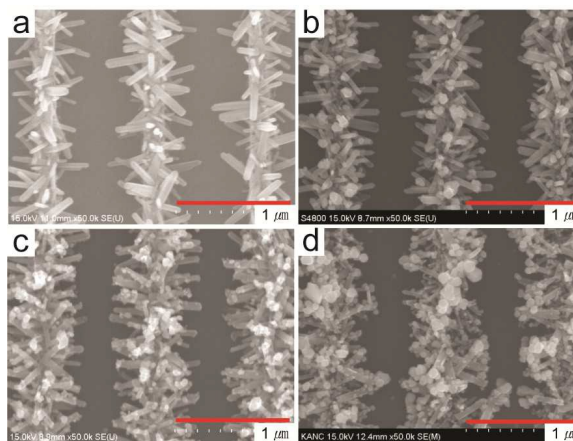
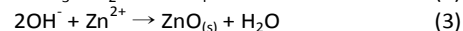
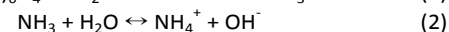


Fig. 3 Top-view SEM images of the Ag NPs-decorated ZnO nanorod arrays with different UV-irradiation times: (a) 0, (b) 15, (c) 30 and (d) 45 min, respectively.

water, leading to the formation of hydroxyl ions that further react with Zn $^{2+}$ ions to form ZnO. This can be summarized in the following equations:



The top-view SEM images of Ag NPs-decorated ZnO nanorod arrays with different UV-irradiation times (i.e., 15, 30 and 45 min) on p-Si (100) are shown in Fig. 3 b-d. Note that the growth conditions of ZnO nanorod arrays are identical for all samples. For the UV-irradiation times of 15, 30 and 45 min, the average diameter of Ag NPs on the ZnO nanorods was found to be 30, 42 and 82 nm, respectively, measured from the images in Fig. 3b-d (see ESI, Fig. S1). The average diameters of the Ag NPs increase with the UV-irradiation time, which is in agreement with the analysis of the UV-visible spectra of Ag

precursor solution by UV irradiation. Interestingly, we noticed that the Ag NPs preferentially attached to ZnO nanorods, but not the Si substrate.

The mechanism for the formation of Ag NPs on ZnO nanostructures by photochemical reduction in the presence of a Ag precursor solution has been rarely reported. Based on our experimental results, we hope the following discussion could help propose a deposition mechanism of Ag NPs on ZnO nanorods for our case. From the photochemical experiments with the Ag precursor solution, it can be revealed that citrate ions are an efficient reductant of silver ions in the presence of UV light. No additional reductant and/or stabilizer is required for the synthesis of Ag NPs on the ZnO nanorod arrays. In order to confirm the importance of citrate ions in the photochemical formation of Ag NPs, a Ag precursor solution was made without citrate, and irradiated by the same UV light for 45 min in the presence of ZnO nanorod arrays. No change was observed in the UV-visible spectrum of the Ag precursor solution after 45 min irradiation. In addition, no Ag NPs were found on the ZnO nanorod arrays. Therefore, it can be inferred that citrate ions played a crucial role for the synthesis of Ag NPs on ZnO nanorod arrays. The decomposition of citrate ions under UV irradiation can be described through the following reaction.^{34,35}



As shown in Eq. (4), acetone-1,3-dicarboxylate, carbon dioxide, H^+ , and electrons are formed due to the photochemical decomposition of citrate. It has been known that citrate could form complex with Ag^+ ions.³⁶ The complexation provides a pathway for Ag^+ ions to receive electrons as a result of photochemical reduction during UV irradiation. The reduced Ag atoms can nucleate into Ag NPs either homogeneously in the solution, stabilized by citrate ions as the capping agent, or heterogeneously on a proper surface. Usually homogeneous nucleation of solid phases requires a higher activation energy barrier and consequently heterogeneous nucleation is more favorable.^{37,38} A lower interfacial energy between the nuclei and a foreign surface means a stronger driving force of heterogeneous nucleation, while this is dependent of the structure and chemistry of the foreign surface.³⁸ In our case, when the ZnO nanorod arrays on Si substrate are exposed to the Ag precursor solution under UV irradiation, two types of foreign surfaces are present, i.e. ZnO and Si. Regardless of the crystallinity of the ZnO, its hydrophobic nature and complexation with citrate ions both facilitate the reduction and nucleation of Ag. Therefore, the ZnO nanorods provide preferred surfaces for Ag NPs to attach.

Based on the above analyses, a mechanism is proposed for the formation of the Ag NPs-decorated ZnO nanorods, as shown in Fig. 4. In Fig. 4, a citrate ion that coordinates with both Zn on a ZnO nanorod surface and Ag ions is highlighted to illustrate the possible mechanism that leads to the preferential growth of Ag NPs on ZnO nanorods. Upon absorption of a photon during UV irradiation, photon excitation happens on a carboxylic group coordinating to Ag^+ ions through a ligand to

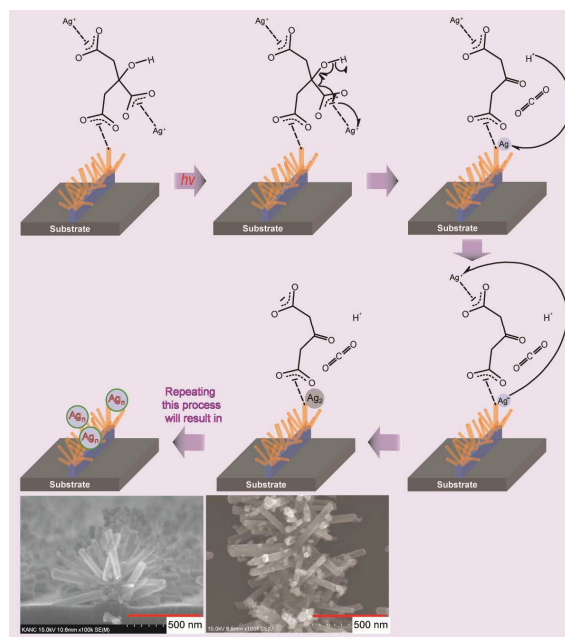


Fig. 4 A proposed mechanism of the formation of the Ag NPs on ZnO nanorods by photochemical reduction. Tilt-view and Top-view SEM images of the Ag NPs-decorated ZnO nanorod arrays from 30 min UV irradiation.

metal charge transfer (LMCT) process,³⁹ where the reduction of a Ag^+ ion occurs and a neutral Ag atom is formed. The unstable citrate radical further undergoes photochemical and thermal decomposition, leading to the formation of a CO_2 and a H^{\bullet} radical, which is in the close proximity to the neutral Ag atom, which more possibly attaches to the ZnO surface than stays in the solution. The H^{\bullet} radical can very likely encounter the neutral Ag atom, the ZnO surface, or another Ag^+ , resulting in the release of an electron and the formation of a H^+ . As a result, two Ag atoms will form after the decomposition of one citrate ion, starting to form a Ag nucleus. The formation of H^+ are generally proposed in various mechanisms for the reduction of Ag^+ .³⁶ However, our study on pH of the synthetic solution did not show a noticeable decrease of pH value. Presumably, H^+ produced in the synthetic solution combined with citrate ion to form citrate acid, resulting in the formation of a citrate/citric acid buffer that stabilizes the pH of the solution. Repeat of the above-described photochemical process leads to the formation of more Ag nuclei and the continuous growth of Ag nuclei. With the assistance of the citrate ions coordinated on ZnO, the Ag nuclei preferentially bond to the ZnO nanorods and further grow into Ag NPs of various sizes, leading to the Ag NPs-decorated ZnO nanorod arrays on Si substrate. This assembly of the Ag NPs on the position-controlled ZnO nanorods was found to be non-uniform and non-specific to any ZnO facets, as shown in Fig. 3b-d. Larger diameter and higher population of Ag NPs are attached to the tip than the root of ZnO nanorods. This is presumably due to the spatial hindrance near the root region.

In order to obtain detailed information of the nanostructure and morphology of Ag NPs-decorated ZnO

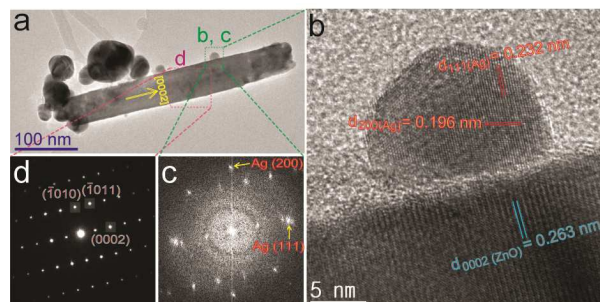


Fig. 5 (a) TEM image of a Ag NPs-decorated ZnO nanorod from 30 min UV irradiation. (b) HR-TEM image of the Ag-ZnO interface and its corresponding (c) FFT image. (d) SAED image taken from the un-decorated ZnO area.

nanorods, TEM analysis was carried out using the sample with 30 min UV irradiation. The obtained bright field TEM image (Fig. 5a) shows that more and larger Ag NPs are attached to the tip than the root of a ZnO nanorod. The observation of a few 30~40 nm Ag NPs and a ~70 nm Ag NPs agrees with the size distribution (see Fig. S2) obtained by measuring with SEM images. Ag NPs of 10 nm and smaller are clearly observed in the TEM image, confirming the presence of tiny Ag NPs that were missed in the size distribution histogram due to the fact that these tiny particles are not easily observed in the SEM images. High-resolution (HR)-TEM and fast Fourier transform (FFT) images of a Ag-ZnO interface area (highlighted in the green box in Fig. 5a), and selected area electron diffraction (SAED) image of an area of ZnO without Ag NP decoration (highlighted in the purple box in Fig. 5a) are also shown in Fig. 5. The HR-TEM image (Fig. 5b) and its FFT image (Fig. 5c) reveal the single crystalline nature of both the ZnO nanorod and the imaged Ag NP. The SAED image of the ZnO nanorod is shown in Fig. 5d for clarity and resolving the crystal orientation. The fringes along the axial direction of the ZnO nanorod have a spacing of 0.263 nm, which can be assigned to the (0002) planes of wurtzite ZnO, indicating that the [0002] is the growth direction of the single crystalline ZnO nanorod. The fringes from the Ag NP have spacing of 0.232 nm and 0.196 nm in agreement with (111) and (200) planes of Ag.^{40,41} Due to the small structure mismatch (2.68%) between the (0002) planes of ZnO and the (111) planes of Ag,⁴² the Ag NP shows an epitaxial growth nature on the sidewall of the ZnO nanorod, with Ag (111) planes almost growing in the same direction as the ZnO (0002) planes. This evidences the direct photochemical deposition on ZnO nanorod surfaces. However, majority of the Ag NPs, especially the larger ones, don't show epitaxial growth nature on the ZnO nanorods. For these larger Ag NPs, we believe they form by the preferential aggregation of Ag nuclei/NPs produced in the solution on the ZnO nanorod surfaces. In addition to their reducing property, the citrate ions are believed to play an important role in grafting the Ag nuclei/NPs on ZnO surface here. Z. R. Tian *et al.* reported that citrate ions adsorb preferentially on the (0002) surface of ZnO.⁴³ In our case, the citrate ions could assist the preferential growth of Ag on the (0002) surfaces of ZnO, which could

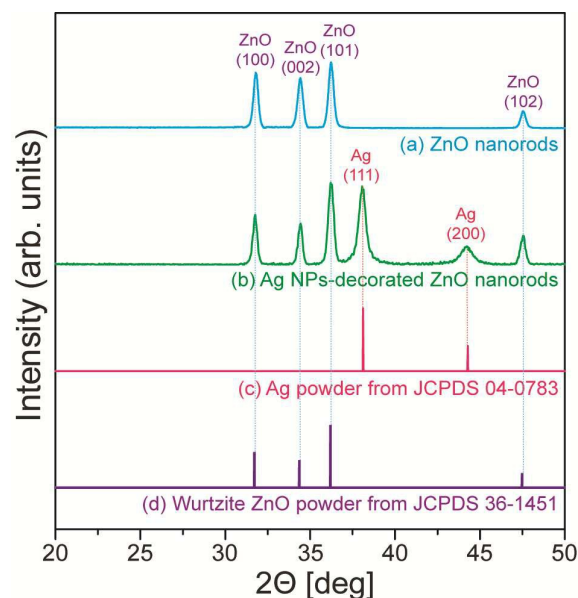


Fig. 6 XRD spectra of (a) ZnO nanorods, (b) Ag NPs-decorated ZnO nanorods with 30 min UV irradiation, reference data of (c) Ag powder from JCPDS 04-0783 and (d) wurtzite ZnO powder from JCPDS 36-1451.

partially contribute to the higher population and larger Ag NPs at the tip of the ZnO nanorods.

XRD was used to investigate the crystallinity of both the non-decorated ZnO nanorods and the Ag NPs decorated ZnO nanorods obtained with 30 min UV irradiation. The corresponding XRD patterns are shown in Fig. 6. All the observed diffraction peaks can be indexed to hexagonal wurtzite ZnO (JCPDS 36-1451) and face-centered cubic (fcc) Ag crystals (JCPDS 04-0783), indicating that the products contain crystalline wurtzite ZnO and Ag.^{44,45} No remarkable shifts of any ZnO diffraction peaks are detected for the Ag NPs-decorated ZnO nanorods, indicating that the photochemical process did not cause noticeable change in the lattice parameters of the ZnO nanorods. However, relatively stronger intensity is observed for the ZnO (101) and (102) diffraction peaks for the Ag NPs decorated ZnO nanorods. This could be due to the epitaxial growth of some Ag NPs on the ZnO nanorod sidewall where the ZnO (101) and (102) facets interface with Ag (200).

In order to investigate the effect of Ag NPs obtained with different UV-irradiation times on the optical properties of ZnO nanorods, PL spectra were measured for the ZnO nanorods with and without Ag NP decoration at room temperature, as shown in Fig. 7. The spectrum from ZnO nanorods without Ag NPs shows a typical broad-band yellow-green emission of ZnO with a strong near band edge (NBE) emission at ~ 3.25 eV and a peak at ~ 1.65 eV that results from the second-order feature of the NBE emission of ZnO.^{46,47} The broad-band emission contains the yellow emission in the range of 2.0 – 2.18 eV and the green emission in the range 2.34 – 2.53 eV that are generally related to a complex of intrinsic defects such as oxygen/zinc vacancies and oxygen/zinc interstitials.⁴⁸ The PL

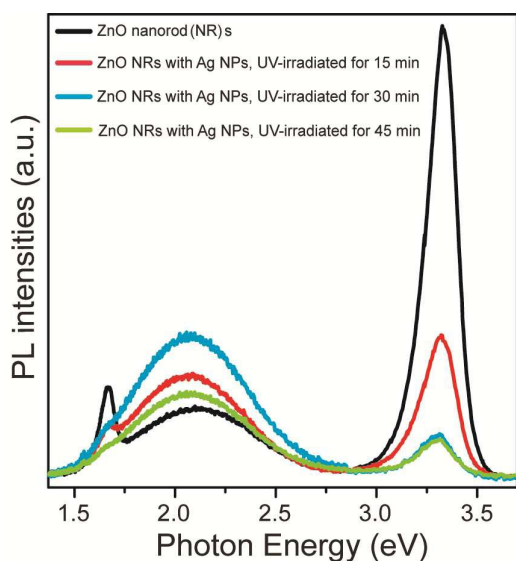


Fig. 7 PL spectra of Ag NPs-decorated ZnO nanorods with different UV-irradiation times.

Table 1 Ratio of the visible emission to the UV emission of Ag-ZnO hybrids and the enhancement rate for Ag-ZnO hybrids, compared with the ZnO nanorods without Ag decoration.

UV-irradiation time (min)	Ratio of visible emission to UV emission	Enhancement rate of Ag-ZnO hybrids, compared with the ZnO nanorods without Ag decoration
0	0.16	-
15	0.72	4.5
30	3.28	20.5
45	2.21	13.8

spectra from the Ag NPs decorated ZnO nanorods show similar ZnO PL characteristics, except that the ratios between different emissions have substantial changes. In Table 1, the ratios of the visible emission to the UV emission of the Ag NPs-decorated ZnO nanorod arrays with different UV-irradiation times are listed. It can be observed in Fig. 7 that the yellow-green emission of the Ag NPs-decorated ZnO nanorod arrays increases remarkably up to the UV-irradiation for 30 min, then decreases substantially at 45 min UV irradiation. This non-monotonic change in the intensity of the yellow-green emission with regards to the increase in the UV-irradiation time indicates that the visible PL intensity might be related to other factors in addition to the oxygen/zinc defects possibly created in ZnO by UV irradiation.

To further understand the influence of Ag NPs on the PL properties of ZnO nanorods, finite difference time domain (FDTD) simulations were performed on the Ag-ZnO hybrid material using Lumerical FDTD Solutions version 8.7.4 (Lumerical Solutions, Vancouver, BC, Canada), as shown in Fig. 8. The simulations were carried out using the average dimensions of Ag NPs and ZnO nanorods obtained from the

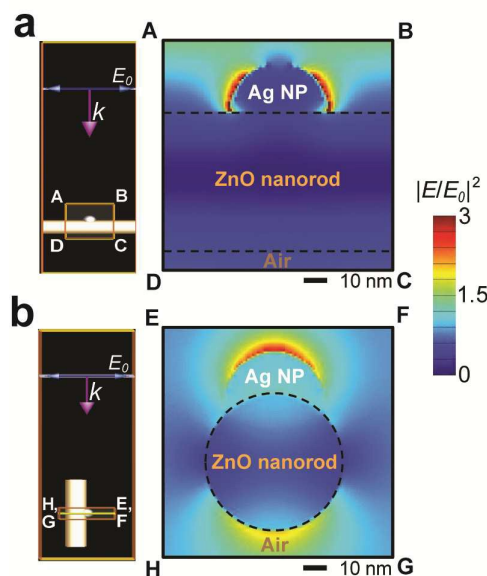


Fig. 8 Simulated electric field intensity distributions in the Ag-ZnO hybrid material, under illumination of linearly polarized plane waves (wavelength: 266 nm). The propagation direction of the incident light is (a) perpendicular and (b) parallel to the axial direction of the ZnO nanorod in the two distributions, respectively. The schematic diagrams on the left of the distributions illustrate the cross-sectional planes, where the field intensity distributions are obtained, and the FDTD simulation configurations. E_0 indicates the magnitude of the electric field of the incident light and k indicates the propagation direction.

sample with 30 min UV irradiation due to the highest value for the ratio of the visible emission to the UV emission among experimental conditions. Namely, the average diameter and length of ZnO nanorods used in the calculation were 58 nm and 294 nm, respectively, where the average diameter of Ag NPs was 42 nm. For simplicity and clarity, the field intensity distributions were obtained for a ZnO nanorod decorated with one hemispherical Ag NP illuminated by a linearly polarized plane wave with a wavelength of 266 nm. Fig. 8a and 8b show exemplary distributions, where the propagation direction of the incident light is perpendicular and parallel to the axial direction of the ZnO nanorod, respectively. In both cases, strong field enhancement can be observed on the Ag NP. This apparently shows that Ag NPs act as efficiently radiative antennas coupling incident light to surface plasmons (SPs).⁴⁹

In our case, the increase in the ratio of the visible emission to the UV emission could be attributed to SP-mediated emission, in which the deep level emission within ZnO nanorods could be coupled into the SP modes of the Ag NPs on ZnO nanorods when the excited energy and the SP energy are similar. As a result of the decoration of Ag NPs, the UV emission intensity of ZnO nanorods is reduced but the visible emission is enhanced. From 0 to 30 min, longer UV irradiation time results in a monotonic increase in this ratio, presumably due to the incorporation of more Ag NPs on ZnO nanorods, i.e., the increase of radiative antennas. However, for the Ag NPs-decorated ZnO nanorod arrays irradiated for 45 min, the ratio of the visible emission to the UV emission becomes decreased, possibly due to segregation of Ag NPs indicated by

the serious broadening in the particle size distribution when compared with the sample irradiated for 30 min (see ESI, Fig. S2). Since the ZnO nanorods have an average diameter of 58 nm, Ag NPs comparable to or smaller than this value can fit on the ZnO nanorods to contribute to increasing the population of Ag NPs in this size range. Presumably high population of smaller Ag NPs on ZnO nanorods leads to a higher probability of coupling, and thus higher SPR energies. However, when the size of Ag NPs is bigger than 58 nm, e.g. when Ag NPs start clustering and form bigger ones, loading more Ag to the sample will not help increase the population of Ag NP antennas. Therefore, among the experimental conditions examined in this paper, 30 min UV irradiation is optimal, where the ratio of the visible emission to the UV emission of ZnO nanorod arrays was increased by 20.5 times *via* introducing SP coupling by Ag NP decoration. In addition, with the increase in the UV-irradiation time, the UV emission at ~ 3.25 eV decreases monotonically. It could be attributed to the improved recombination rate of the deep level emission due to the coupling of the emission with SPs of the Ag NPs on ZnO surface. The recombination rate is enhanced by the ZnO-SP coupling rate, which is expected to be very fast compared to the radiative and nonradiative recombination rates.⁵⁰ As results, the UV emission is quenched while the visible emission improved. Such enhanced emission properties of the Ag NPs-decorated ZnO nanorod arrays can be optimized for specific intended applications such as compact optical devices.

Conclusions

We demonstrated a novel technique for the position-controlled growth of ZnO nanorods decorated with Ag NPs by combining UV-NIL, hydrothermal growth and photochemical method. By controlling the UV-irradiation time, Ag NPs of various size distributions can be selectively deposited on ZnO nanorods. Due to the small structure mismatch between the (0002) planes of ZnO and the (111) planes of Ag, and also the preferential adsorption of citrate ions on the (0002) surface of ZnO, the tip of ZnO nanorods is more populated with Ag NPs. Epitaxial growth of Ag NPs is also observed on the sidewall of ZnO nanorods. Tuning the ratio of the visible emission to the UV emission of ZnO nanorods can be realized by varying the UV irradiation time, i.e., varying the resultant size contribution of Ag NPs on ZnO nanorods. The ratio of the visible emission to the UV emission of the ZnO nanorod arrays was increased by 20.5 times by introducing Ag NPs by photochemical reduction. The decoration of ZnO with Ag NPs has been known to be an effective strategy to enhance the light emission properties, in which the interaction between ZnO and Ag is dominated by the size distribution of Ag NPs *via* SP coupling. The technique demonstrated here offers an alternative approach to the Ag NPs-decorated ZnO nanorod arrays and, it is compatible with the low-temperature fabrication (120 °C and lower) on flexible substrates. Also, the attached Ag NPs can be further functionalized and conjugated with various molecules for a broader property tuning. The Ag NPs-decorated ZnO nanorod

arrays may find applications such as chemical and biological sensors.

Acknowledgement

This research was supported by Nano · Material Technology Development Program through the National Research Foundation of Korea (NRF) funded by the Ministry of Science, ICT and Future Planning (2015M3A7B7044548).

Notes and references

- 1 T. Dufaux, J. Dorfmueller, R. Vogelgesang, M. Burghard and K. Kern, *Appl. Phys. Lett.*, 2010, **97**, 161110.
- 2 B. J. Lawrie, J.-W. Kim, D. P. Norton and R. F. Haglund, *Nano Lett.*, 2012, **12**, 6152.
- 3 H.-Y. Chen, K.-W. Liu, M.-M. Jiang, Z.-Z. Zhang, L. Liu, B.-H. Li, X.-H. Xie, F. Wang, D.-X. Zhao, C.-X. Shan and D.-Z. Shen, *J. Phys. Chem. C*, 2014, **118**, 679.
- 4 X. Cui, K. Tawa, K. Kintaka and J. Nishii, *Adv. Funct. Mater.*, 2010, **20**, 945.
- 5 M.-C. Jeong, B.-Y. Oh, M.-H. Ham and J.-M. Myung, *Appl. Phys. Lett.*, 2006, **88**, 202105.
- 6 R. Könenkamp, R. C. Word and C. Schlegel, *Appl. Phys. Lett.*, 2004, **85**, 6004.
- 7 M. H. Huang, S. Mao, H. Feick, H. Yan, Y. Wu, H. Kind, E. Weber, R. Russo and P. Yang, *Science*, 2001, **292**, 1897.
- 8 P. Yang, H. Yan, S. Mao, R. Russo, J. Johnson, R. Saykally, N. Morris, J. Pham, R. He and H.-J. Choi, *Adv. Funct. Mater.*, 2002, **12**, 323.
- 9 Z. L. Wang and J. Song, *Science*, 2006, **312**, 242.
- 10 J. Jean, S. Chang, P. R. Brown, J. J. Cheng, P. H. Rekemeyer, M. G. Bawendi, S. Gradečak and V. Bulović, *Adv. Mater.*, 2013, **25**, 2790.
- 11 J. X. Wang, X. W. Sun, Y. Yang, H. Huang, Y. C. Lee, O. L. Tan and L. Vayssieres, *Nanotechnology*, 2006, **17**, 4995.
- 12 X. Wang, C. J. Summers and Z. L. Wang, *Nano Lett.*, 2004, **4**, 423.
- 13 H. Kim, M. Osofsky, S. M. Prokes, O. J. Glembocki and A. Piqué, *Appl. Phys. Lett.*, 2013, **102**, 171103.
- 14 G. V. Naik, V. M. Shalaev and A. Boltasseva, *Adv. Mater.*, 2013, **25**, 3264.
- 15 M. Rycenga, C. M. Cobley, J. Zeng, W. Li, C. H. Moran, Q. Zhang, D. Qin and Y. Xia, *Chem. Rev.*, 2011, **111**, 3669.
- 16 Y. Chen, W. H. Tse, L. Chen and J. Zhang, *Nanoscale Res. Lett.*, 2015, **10**, 106.
- 17 H. Tang, G. Meng, Q. Huang, Z. Zhang, Z. Huang and C. Zhu, *Adv. Fun. Mater.*, 2012, **22**, 218.
- 18 Q. Tao, S. Li, C. Ma, K. Liu and Q.-Y. Zhang, *Dalton Trans.*, 2015, **44**, 3447.
- 19 Y. Wei, J. Kong, L. Yang, L. Ke, H. R. Tan, H. Liu, Y. Huang, X. W. Sun, X. Lu and H. Du, *J. Mater. Chem. A*, **1**, 5045.
- 20 D. D. Lin, H. Wu, R. Zhang and W. Pan, *Chem. Mater.*, 2009, **21**, 3479.
- 21 N. L. Tarwal and P. S. Patil, *Electrochim. Acta*, 2011, **56**, 6510.
- 22 H. R. Liu, G. X. Shao, J. F. Zhao, Z. X. Zhang, Y. Zhang, J. Liang, X. G. Liu, H. S. Jia and B. S. Xu, *J. Phys. Chem. C*, 2012, **116**, 16182.
- 23 C. Ren, B. Yang, M. Wu, J. Xu, Z. Fu, Y. Iv, T. Guo, Y. Zhao and C. Zhu, *J. Hazard. Mater.*, 2010, **182**, 123.
- 24 M. Macias-Montero, A. Borrás, Z. Saghi, P. Romero-Gomez, J. R. Sanchez-Valencia, J. C. Gonzalez, A. Barranco, P. Midgley, J. Cotrino and A. R. Gonzalez-Elipe, *J. Mater. Chem.*, 2012, **22**, 1341.

ARTICLE

Nanoscale

- 25 K. Zhong, Y. C. Mao, X. F. Sun, C. L. Liang, P. Liu and Y. X. Tong, *J. Electrochem. Soc.*, 2012, **159**, K161.
- 26 X. T. Yin, W. X. Que, D. Fei, F. Y. Shen and Q. S. Guo, *J. Alloys Compd.*, 2012, **524**, 13.
- 27 Y. F. Wei, L. Ke, J. H. Kong, H. Liu, Z. H. Jiao, X. H. Lu, H. J. Du and X. W. Sun, *Nanotechnology*, 2012, **23**, 235401.
- 28 H.-H. Park, X. Zhang, K. W. Lee, K. H. Kim, S. H. Jung, D. S. Park, Y. S. Choi, H.-B. Shin, H. K. Sung, K. H. Park, H. K. Kang, H.-H. Park and C. K. Ko, *CrystEngComm*, 2013, **15**, 3463.
- 29 S. J. Choi, P. J. Yoo, S. J. Beak, T. W. Kim and H. H. Lee, *J. Am. Chem. Soc.*, 2004, **126**, 7744.
- 30 K. Y. Suh, H. E. Jeong, D.-H. Kim, R. A. Singh and E.-S. Yoon, *J. Appl. Phys.*, 2006, **100**, 034303.
- 31 S. Agnihotri, S. Mukherji and S. Mukherji, *RSC Adv.*, 2014, **4**, 3974.
- 32 Z. Zhou and Y. Deng, *J. Phys. Chem. C*, 2009, **113**, 19853.
- 33 S. Baruah and J. Dutta, *Sci. Technol. Adv. Mater.*, 2009, **10**, 013001.
- 34 M. Maillard, P. Huang and L. Brus, *Nano Lett.*, 2003, **3**, 1611.
- 35 R. L. Redmond, X. Wu and L. Brus, *J. Phys. Chem. C*, 2007, **111**, 8942.
- 36 A. Henglein and M. Giersig, *J. Phys. Chem. B*, 1999, **103**, 9533.
- 37 X. Y. Liu, *J. Cryst. Growth*, 2002, **237–239**, 1806.
- 38 F. Scholz, *Electrochem. Commun.*, 2011, **13**, 932.
- 39 C. H. Munro, W. E. Smith, M. Garner, J. Clackson and P. C. White, *Langmuir*, 1995, **11**, 3712.
- 40 X. C. Jiang, S. X. Xiong, Z. A. Tian, C. Y. Chen, W. M. Chen and A. B. Yu, *J. Phys. Chem. C*, 2011, **115**, 1800.
- 41 E. A. Owen and G. I. Williams, *J. Sci. Instrum.*, 1954, **31**, 49.
- 42 S. Wang, Y. Yu, Y. Zuo, C. Li, J. Yang and C. Lu, *Nanoscale*, 2012, **4**, 5895.
- 43 Z. R. Tian, J. A. Voigt, J. Liu, B. Mckenzie, M. J. Mcdermott, M. A. Rodriguez, H. Konishi and H. Xu, *Nature Mater.*, 2003, **2**, 821.
- 44 B. Cao and W. Cai, *J. Phys. Chem. C*, 2008, **112**, 680.
- 45 Y. Fu, L. Liu, L. Zhang and W. Wang, *ACS Appl. Mater. Interfaces*, 2014, **6**, 5105.
- 46 F. Fabbri, M. Villani, A. Catellani, A. Calzolari, G. Cicero, D. Calestani, G. Calestani, A. Zappettini, B. Dierre, T. Sekiguchi and G. Salviati, *Sci. Rep.*, 2014, **4**, 5158.
- 47 Y. G. Wang, S. P. Lau, X. H. Zhang, H. H. Hng, H. W. Lee, S. F. Yu and B. K. Tay, *J. Cryst. Growth*, 2003, **259**, 335.
- 48 H. S. Kang, J. W. Kim, S. H. Lim, H. W. Chang, G. H. Kim, J. H. Kim, S. Y. Lee, *Superlattices Microstruct.*, 2006, **39**, 193.
- 49 I. Gontijo, M. Boroditsky, E. Yablonovitch, S. Keller, U. K. Mishra and S. P. DenBaars, *Phys. Rev. B: Condens. Matter*, 1999, **60**, 11564.
- 50 C. K. Choi, Y. H. Kwon, B. D. Little, G. H. Gainer, J. J. Song, Y. C. Chang, S. Keller, U. K. Mishra and S. P. DenBaars, *Phys. Rev. B: Condens. Matter*, 2001, **64**, 245339.